Mott phases and superfluid-insulator transition of dipolar spin-three bosons in an optical lattice: implications for ^{52}Cr atoms

Jean-Sébastien Bernier,[1] K. Sengupta,[2] and Yong Baek Kim[1, 3, 4]

[1] *Department of Physics, University of Toronto, Toronto, Ontario, Canada M5S 1A7*
[2] *TCMP Division, Saha Institute of Nuclear Physics, 1/AF Bidhannagar, Kolkata-700064, India*
[3] *School of Physics, Korea Institute for Advanced Study, Seoul 130-722, Korea*
[4] *Department of Physics, University of California, Berkeley, California 94720*

(Dated: February 6, 2008)

We study the Mott phases and superfluid-insulator transition of spin-three bosons in an optical lattice with an anisotropic two dimensional optical trap. We chart out the phase diagrams for Mott states with $n = 1$ and $n = 2$ atoms per lattice site. It is shown that the long-range dipolar interaction stabilizes a state where the chains of the ferromagnetically aligned spins run along the longer trap direction while the spin ordering is staggered between nearby chains, leading to an antiferromagnetic ordering along the shorter trap direction. We also obtain the mean-field phase boundary for the superfluid-insulator transition in these systems and study the nature of spin ordering in the superfluid state near the transition. We show that, inside the superfluid phase and near the superfluid-insulator phase boundary, the system undergoes a first order antiferromagnetic-ferromagnetic spin ordering transition. We discuss implications of our results for ^{52}Cr atoms and suggest possible experiments to detect different phases in such systems.

PACS numbers:

I. INTRODUCTION

Several experiments on ultracold trapped atomic gases have opened a new window onto a plethora of intriguing phases of quantum matter.[1,2] A gas of bosonic atoms in an optical or magnetic trap has been reversibly tuned between superfluid (SF) and insulating ground states by varying the strength of a periodic potential produced by standing optical waves. This transition has been explained on the basis of the Bose-Hubbard model with on-site repulsive interactions and hopping between nearest neighboring sites of the lattice[3]. As long as the atom-atom interactions are small compared to the hopping amplitude, the ground state remains superfluid. In the opposite limit of a strong lattice potential, the interaction energy dominates and the ground state is a Mott insulator (MI) when the density is commensurate, with an integer number of atoms localized at each lattice site.

In the above-mentioned experiments, the spins of the atoms were neglected either due to freezing of the spin degrees of freedom in the presence of a magnetic trap or due to the use of spinless atoms. Later, use of optical trap for confining atoms led to realization of spin-one and spin-two bosonic systems where the spins of the atoms are dynamical degrees of freedom[4,5]. Furthermore, possibilities of creating two-component bosonic mixture, which is equivalent to bosons with pseudospin half, has also been discussed[6]. In all of these systems, the bosonic atoms are shown to have spin-dependent contact interaction which can lead to variety of spin ordered Mott ground states[6,7,8,9,10,11]. The superfluid-insulator transitions in these systems has also been studied[7,9,11,12].

More recently, a Bose-Einstein condensate of ^{52}Cr atoms has been realized[13]. These Cr atoms, in contrast to their alkali counterparts, have the electronic configuration $[Ar]\, 3d^5\, 4s^1$ which leads, for the isotopes with no nuclear spin, to a net spin of 3 (in units of $\hbar$) and to a magnetic moment of $6\mu_B$, where μ_B is the Bohr magneton[14]. Consequently, these atoms experience a much stronger long-range dipolar interaction compared to their alkali counterparts. Besides, again in stark contrast to other bosonic alkali atoms, in a Cr condensate, the scattering lengths in different angular momentum channel are quite different[15]. Since the Cr atoms have spin 3, the relevant scattering lengths (a_S) occurs in angular momentum channels $S = 0, 2, 4, 6$. All the a_S except a_0 are determined and have the values $a_2 = -7a_B$, $a_4 = 58a_B$ and $a_6 = 112a_B$, where a_B is the Bohr radius[14,15]. Such different scattering lengths lead to much stronger spin-dependent contact interaction potentials in Cr compared to its alkali counterparts[15]. In fact, in the presence of an optical trap, where the spins become dynamical degrees of freedoms, the spin-dependent contact interactions overwhelm the long-ranged dipolar interaction energy, and lead to various spin-nematic phases[15,16]. In particular, it has been predicted in Ref. 15 that biaxial nematic phases may be realized in Cr condensates[17].

In this work, we study the Mott phases and superfluid-insulator transition of spin-three bosons in an optical lattice with an anisotropic two dimensional optical trap. The main results reported in this paper are as follows. First, we map out the phase diagrams for Mott states with $n = 1$ and $n = 2$ atoms per lattice site. In particular, we demonstrate that both the contact and the dipolar interactions are important for obtaining the correct Mott ground states. It is shown that the presence of a long-range dipolar interaction and an anisotropic two-dimensional (2D) trap lead to a Mott ground state where the chains of the ferromagnetically (FM) aligned spins run along the longer trap direction while the spin order-

ing is staggered between nearby chains, leading to an antiferromagnetic (AFM) ordering along the shorter trap direction. Second, we obtain the superfluid-insulator transition (SIT) phase boundary of this system using mean-field theory and discuss the spin ordering of the superfluid near and away from the transition. We demonstrate that, in contrast to the alkali bosonic atoms with weak spin-dependent contact interaction and negligible dipolar interactions, the spin-three bosons with dipolar interaction exhibit a first order AFM-FM transition for the spin ordering in the condensate as one moves away from the SIT boundary into the superfluid phases. Finally, we suggest future experiments on ^{52}Cr to test our theoretical predictions.

We start with the following Hamiltonian

$$\mathcal{H} = \mathcal{H}'_K + \mathcal{H}'_O + \mathcal{H}'_D \quad (1)$$

$$\mathcal{H}'_K = \int d\mathbf{r}\ \hat{\psi}^\dagger_a(\mathbf{r}) \left(-\frac{\hbar^2}{2M}\nabla^2 + V(\mathbf{r})\right) \hat{\psi}_a(\mathbf{r}) \quad (2)$$

$$\mathcal{H}'_O = \frac{1}{2}\int d\mathbf{r}\ d\mathbf{r}' \hat{\psi}^\dagger_a(\mathbf{r})\hat{\psi}^\dagger_{a'}(\mathbf{r}')u(\mathbf{r}-\mathbf{r}')\hat{\psi}_{b'}(\mathbf{r}')\hat{\psi}_b(\mathbf{r}) \quad (3)$$

$$\mathcal{H}'_D = \frac{u_4}{2}\int d\mathbf{r}\ d\mathbf{r}' \hat{\psi}^\dagger_a(\mathbf{r})\hat{\psi}^\dagger_{a'}(\mathbf{r}') \left(\frac{\mathbf{S}_{ab}\cdot\mathbf{S}_{a'b'}}{|\mathbf{r}-\mathbf{r}'|^3} - 3\ S^u_{ab}\ S^v_{a'b'}\ \frac{(\mathbf{r}-\mathbf{r}')_u\ (\mathbf{r}-\mathbf{r}')_v}{|\mathbf{r}-\mathbf{r}'|^5}\right) \hat{\psi}_{b'}(\mathbf{r}')\hat{\psi}_b(\mathbf{r}), \quad (4)$$

where $\hat{\psi}^\dagger_a(\mathbf{r})$ is the boson creation operator with spin projection $a = \{-3,-2,-1,0,1,2,3\}$ at position $\mathbf{r}$, $V(\mathbf{r})$ is the optical lattice potential, S^u_{ab} denotes the element of the three spin-3 rotation matrices, sum over all repeated indices are implied, and $u(\mathbf{r}-\mathbf{r}')$ is the two-body interatomic potential given by

$$u(\mathbf{r}-\mathbf{r}') = \delta(\mathbf{r}-\mathbf{r}')(g_0P_0 + g_2P_2 + g_4P_4 + g_6P_6), \quad (5)$$

where $g_S = 4\pi\hbar^2 a_S/M$ and $P_S = \sum_{m=-S}^{S} |S,m\rangle\langle S,m|$ is the projection operator for the Bosons. Using the identities

$$\begin{aligned} 1 &= P_0 + P_2 + P_4 + P_6, \\ (\mathbf{S}\cdot\mathbf{S}') &= -12P_0 - 9P_2 - 2P_4 + 9P_6, \\ (\mathbf{S}\cdot\mathbf{S}')^2 &= 144P_0 + 81P_2 + 4P_4 + 81P_6, \end{aligned} \quad (6)$$

we can rewrite the contact interaction as

$$u(\mathbf{r}-\mathbf{r}') = \delta(\mathbf{r}-\mathbf{r}')\left[u_0 + u_1P_0 + u_2(\mathbf{S}\cdot\mathbf{S}') + u_3(\mathbf{S}\cdot\mathbf{S}')^2\right], \quad (7)$$

where $u_0 = (-11g_2 + 81g_4 + 7g_6)/77$, $u_1 = g_0 + (-55g_2 + 27g_4 - 5g_6)/33$, $u_2 = (g_6 - g_2)/18$, $u_3 = (g_2/126 - g_4/77 + g_6/198)$. The coefficient of the dipolar term u_4 is known to be small (*i.e.* $u_4 \ll u_0, u_1, u_2, u_3$) in ^{52}Cr atom[15].

For ultracold atoms in an optical lattice, it is well-known that the energy eigenstates are Bloch wave functions and a superposition of these Bloch states yields a set of Wannier functions that are well localized on the individual lattice sites for deep enough lattices[1,18]. Further, in these systems both the kinetic and interaction energies involved in the dynamics are small compared to the excitation energies to higher single particle bands in the limit of deep optical lattices necessary to realize the Mott insulating state[1,18]. We shall therefore expand the boson field operators in the Wannier basis keeping only the lowest single particle band, $\psi_a(\mathbf{r}) = \sum_i b_{ia} w(\mathbf{r}-\mathbf{r}_i)$, where b_{ia} is the spin-3 boson annihilation operator at site i with spin projection a. After a few straightforward manipulations, we then obtain the effective single band extended Bose-Hubbard Hamiltonian on a lattice $\mathcal{H}_B = \mathcal{H}_K + \mathcal{H}_O + \mathcal{H}_D$, where

$$\mathcal{H}_K = -t\sum_{\langle ij\rangle}\sum_a \left(b^\dagger_{ia}b_{ja} + \text{h.c}\right) \quad (8)$$

$$\mathcal{H}_O = \frac{U_0}{2}\sum_i \hat{n}_i(\hat{n}_i - 1) + \frac{U_2}{2}\sum_i (\mathbf{S}_i^2 - 12\ \hat{n}_i) + \frac{U_1}{2}\sum_i\sum_{ab}\frac{1}{7}(-1)^a\ b^\dagger_{ia}\ b^\dagger_{i-a}\ (-1)^b\ b_{ib}\ b_{i-b} + \frac{U_3}{2}\sum_i[\sum_{k,l=\{x,y,z\}} N^2_{i,kl} - 132\ \hat{n}_i] \quad (9)$$

$$\mathcal{H}_D = \frac{U_4}{2}\sum_{i,j}\left(\frac{\mathbf{S}_i\cdot\mathbf{S}_j}{|\mathbf{r}_i-\mathbf{r}_j|^3} - 3\ S^v_i\ S^v_j\frac{(\mathbf{r}_i-\mathbf{r}_j)_u\ (\mathbf{r}_i-\mathbf{r}_j)_v}{|\mathbf{r}_i-\mathbf{r}_j|^5}\right). \quad (10)$$

Here $\hat{n}_i = \sum_a b^\dagger_{ia}b_{ia}$ is the boson density at site i, $\mathbf{S}_i = \sum_{ab} b^\dagger_{ia}\mathbf{S}_{ab}b_{ib}$ is the spin operator and $N_{i,kl} = \sum_{ab} b^\dagger_{ia}(S_kS_l)_{ab}b_{ib}$ is the 'nematic' operator. The hopping coefficient t is given by $t = \int d\mathbf{r}\ w^*(\mathbf{r}-\mathbf{r}_i)\left(-\frac{\hbar^2}{2M}\nabla^2 + V(\mathbf{r})\right)\ w(\mathbf{r}-\mathbf{r}_j)$ and the U's are given by $U_i = u_i\int d\mathbf{r}|w(\mathbf{r})|^4$, for $i = \{0,1,2,3\}$, and $U_4 = u_4\int d\mathbf{r}|w(\mathbf{r})|^2\ \int d\mathbf{r}'|w(\mathbf{r}')|^2$.

The Hamiltonian $\mathcal{H}_B$ is the starting point of our study in the subsequent sections. In what follows, we shall obtain the ground states of $\mathcal{H}_B - \mu\sum_i \hat{n}_i$ as a function of U_1/U_0, U_2/U_0, U_3/U_0, μ/U_0, and t/U_0, where μ denotes the chemical potential for a fixed weak dipolar interaction $U_4/U_0 \ll 1, U_{i=\{1,2,3\}}/U_0$. Note that since the value of a_0 and hence U_1 is not experimentally determined, the position of ^{52}Cr in this generalized phase diagram is not known. However, we expect that some of the general features obtained from this phase diagram will apply to ^{52}Cr. Also, we would like to point out that in principle we expect the chemical potential μ to be space-dependent due to the presence of the trapping potential. In this work, we have ignored this effect of the optical trap which is a standard approximation in the literature for large traps[19].

The rest of the paper is organized as follows. In Sec. II, we study various possible Mott phases of the $\mathcal{H}_B$. This is followed, in Sec. III, by a mean-field study of the SIT in this model. Then in Sec. IV, we suggest experiments to test our predictions. Finally, we conclude in Sec. V.

II. MOTT PHASES

In this section, we obtain various possible Mott phases when there are integer n particles per site. In the Mott limit, the kinetic energy of atoms are negligible and we shall take $t = 0$ in the rest of this section. We shall concern ourselves only with the case of $n = 1$ and $n = 2$ atoms per site in this work. The calculations can be generalized, in principle, to higher n values. The phase diagram for the on-site terms is sketched in Sec. II A while the effect of the dipolar interaction is presented in Sec. II B.

A. On-site Interaction

In order to obtain the Mott phases, we use the fact that the dipolar interaction term $\mathcal{H}_D$ (Eq. 10) is small compared to the on-site interaction terms in $\mathcal{H}_O$ (Eq. 9). Thus, we first neglect the dipole term $\mathcal{H}_D$ and find out the ground-state of $\mathcal{H}_O$ by minimizing the variational energy

$$E_v(n) \;=\; \langle \Psi_v(n)| \, \mathcal{H}_O \, |\Psi_v(n)\rangle \,, \tag{11}$$

where the on-site variational wavefunction $|\Psi_v(n)\rangle$ for n bosons per lattice site is given by

$$|\Psi_v(n)\rangle \;=\; \prod_i \sum_{S=S_{\rm total}} \sum_{m=-S}^{S} c_{i,(n,S,m)} |n;S,m\rangle_i, \tag{12}$$

where $S_{\rm total}$ denotes all the possible total spin that can be obtained by adding spins of n spin-three bosons and m is the azimuthal quantum number corresponding to S. For example for $n = 2$, the possible values of $S_{\rm total} = 0, 2, 4, 6$.

Details of the calculation of $E_v(n)$ are sketched in Appendix A. Here we present the phase diagram obtained by numerical minimization of $E_v(n)$ for $n = 1$ and $n = 2$ as a function of U_3/U_0 and U_2/U_0 for several representative values of μ/U_0 and for $U_1/U_0 = \pm 0.2$. These values of μ and U_1 are chosen for clarity; we have checked that there are no other phases that occur for other values of μ and U_1. In order to find the lower boundary in U_3/U_0 for the $n = 2$ states, we also minimize $E_v(n = 3)$. However, since we are mostly concerned with the $n = 1$ and $n = 2$ states and also for clarity, we have not indicated the different S regions of $n = 3$ in the phase diagrams shown in Figs. 1, 2, 3, and 4. From our calculations, we find that $\mathcal{H}_O$ do not lift the azimuthal degeneracy of the atoms and the ground states obtained from this on-site variational wavefunction are degenerate. The only exception to this occurs for the singlet ground state ($S = 0$) that exists in a narrow region of the phase diagram. For all other phases, the on-site interactions determine only the S value of the ground state, thus leaving a $2S + 1$ degeneracy corresponding to different possible m values. This is where the dipole interaction comes into play. The presence of the dipolar interaction fixes the direction of the spins and gives us a unique ground state. Notice that the weakness of the dipolar interactions compared to the on-site term $\mathcal{H}_O$ ensures that the former would not change the value of S in the ground state.

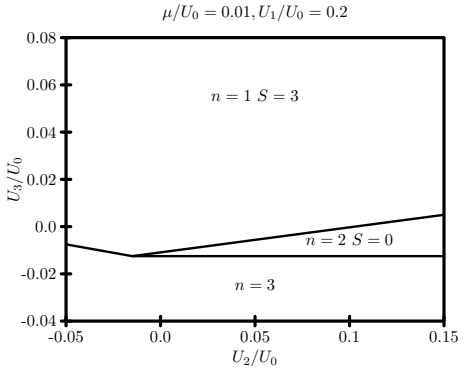

FIG. 1: Mott phase diagram obtained by minimization of $E_v(n)$ for $n = 1$ and $n = 2$ as a function of U_2/U_0 and U_3/U_0 for $\mu = 0.01U_0$ and $U_1/U_0 = 0.2$. Note that the azimuthal degeneracy is not lifted and hence the ground states for non-zero S have a $2S + 1$ fold degeneracy.

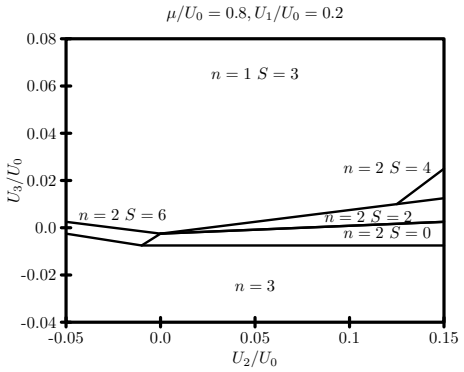

FIG. 2: Same as in Fig. 1 for $\mu = 0.8U_0$ and $U_1/U_0 = 0.2$

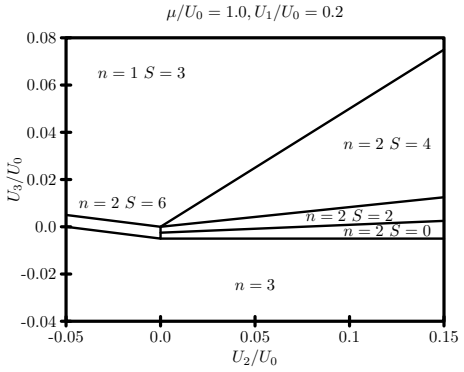

FIG. 3: Same as in Fig. 1 for $\mu = U_0$ and $U_1/U_0 = 0.2$

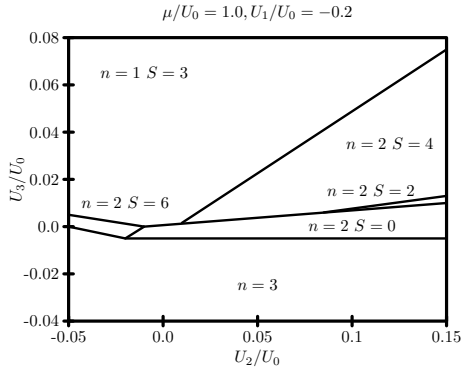

FIG. 4: Same as in Fig. 1 for $\mu = U_0$ and $U_1/U_0 = -0.2$

B. Dipolar Interaction

To investigate the effect of the dipolar interaction, we now restrict ourselves to the lowest S manifold which has been determined by minimizing $E_v(n)$. However, even within this manifold, we need to construct a variational wavefunction to obtain the ground state of $\mathcal{H}_D$. Since the dipole interaction is long-ranged, such a trial wavefunction need not be a simple on-site product wavefunction. To guess the form of this wavefunction, we first look at the dipolar interaction for classical spins in an optical lattice and find out the ground state for such spins. Next, we choose a variational wavefunction which is compatible with the symmetry of this classical ground state.

In the classical limit, the spins can be parameterized as $\mathbf{S}_i = S(\sin\theta_i\cos\phi_i, \sin\theta_i\sin\phi_i, \cos\theta_i)$. Also, due to the form of the dipolar interaction (Eq. 10) and the two-dimensional nature of our system, it is easy to see that the ground state, in the classical limit, shall have all spins aligned in the XY plane. Thus in the ground state, each classical spin can be represented by a single angle ϕ. This simplifies the computational procedure enormously and enables us to study the ground states of classical spins for different trap configurations with both open and periodic boundary conditions.

To find the minimum energy configuration for the classical spins, we minimize $\mathcal{H}_D(\phi_i)$ for both square and rectangular trap geometries. For square traps with open boundary conditions or rectangular traps with periodic boundary conditions in both x and y directions, the bulk region exhibits a swirling pattern described by four interpenetrating sublattices (see Fig.5) with the spins making an angle β with the lattice at each site (see Fig. 6). Moreover, simulations with periodic boundary conditions in both trap directions show that the system energy is degenerate for all values of β. Consequently, for square traps, dipolar interactions are not sufficient to lift the spin degeneracy. However, this situation is difficult to realize in realistic finite size systems with optical traps where a rectangular trap with open boundary condition is a more realistic choice. For the rest of this work, we shall therefore concentrate on such geometries. In this

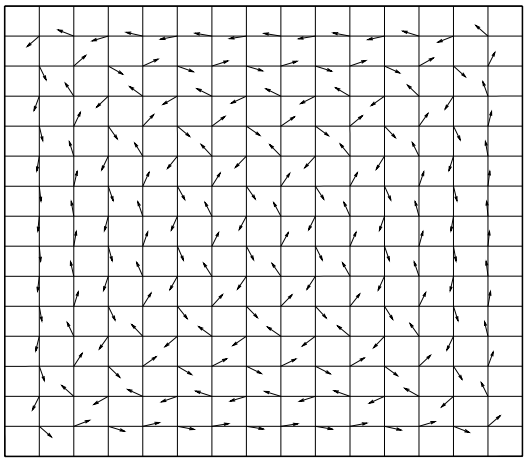

FIG. 5: 14×14 lattice with the open boundary condition. Notice that the spins in the bulk region are following a "swirling" pattern that can be described by four interpenetrating sublattices.

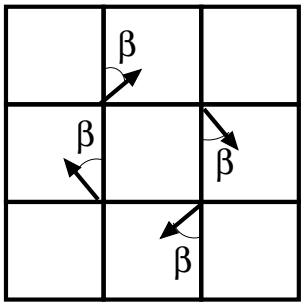

FIG. 6: Typical spin pattern for classical spins with dipolar interactions in the square lattice with the periodic boundary condition. The ground state has infinite degeneracy corresponding to different values of β.

case, the spins of the bulk region tend to align with the longest trap direction as shown in Fig.7. Consequently, in the classical sense, the spin degeneracy is completely lifted by dipolar interactions in rectangular geometries. The ground state for the classical spins for rectangular trap with open boundary condition thus have an antiferromagnetic(AFM) order along the shorter trap direction. Note that such an order corresponds to an interpenetrating four-sublattice structure shown in Fig. 6 with $\beta = \pm\pi/2$ when x is taken as the longest trap direction.

The lesson we learn from the study of the dipolar Hamiltonian in the classical limit is that for rectangular traps with open boundary conditions, the ground state has four interpenetrating sublattices as seen in Fig. 7. Therefore, a reasonable minimal trial wavefunction for finding the ground state of $\mathcal{H}_D$ in the quantum limit must at least have a four-sublattice structure. With this observation, we choose the following variational wavefunction

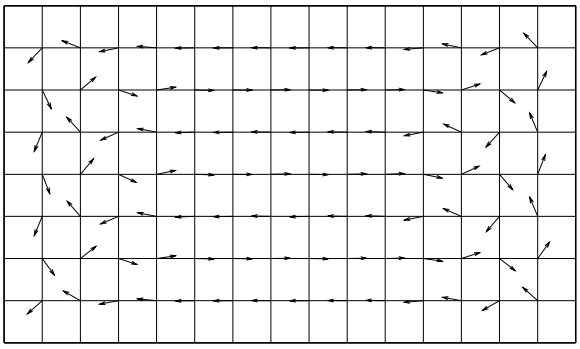

FIG. 7: 14×7 lattice with the open boundary condition. Notice that the spins in the bulk region are aligned along the longer trap direction. This pattern can be described via four interpenetrating sublattices.

for $n = 1$

$$|\Psi_{\rm dipole}(n=1)\rangle \;=\; \prod_{\Lambda=\{A,B,C,D\}} \prod_{i\in\Lambda} \times \sum_{m=-3}^{3} c_{i,(n=1,S=3,m)} |1;3,m\rangle_i, \tag{13}$$

where $\{A, B, C, D\}$ are the four sublattices. Similarly for $n = 2$, one gets

$$|\Psi_{\rm dipole}(n=2)\rangle \;=\; \prod_{\Lambda=\{A,B,C,D\}} \prod_{i\in\Lambda} \times \sum_{S=\{0,2,4,6\}} \sum_{m=-S}^{S} c_{i,(n=2,S,m)} |2;S,m\rangle_i. \tag{14}$$

We then minimize $E_v^{\rm dipole}(n) = \langle\Psi_{\rm dipole}(n)|\,\mathcal{H}_D\,|\Psi_{\rm dipole}(n)\rangle$ to obtain the ground state for the system. We have carried out this numerical minimization for rectangular lattice sizes up to 16×8 with periodic boundary conditions in one of the two directions. For all values of $S \neq 0$ and for all lattice sizes up to 16×8, we find again that the spins are aligned parallel to the longest trap direction and have the same four interpenetrating sublattice structure as shown in Fig. 7. Since this ground state turns out to be generic for all $S \neq 0$, we expect to find such a ground state for ^{52}Cr atoms irrespective of its position in the generalized phase diagram for $n = 1$. For $n = 2$, the ground state will either be the four interpenetrating sublattice structure mentioned previously (if $S \neq 0$) or a singlet (S=0).

III. SUPERFLUID-INSULATOR TRANSITION

A. Phase Boundary

In this section, we obtain the superfluid-insulator phase boundary starting from the $n = 1$ Mott phase within a mean-field theory. To allow density fluctuations in the superfluid state, we construct a variational wavefunction that is a superposition of $n = 0$, $n = 1$ and $n = 2$ Mott states. Note that the variational wavefunction here needs to have the four sublattice structure mentioned in Sec. II B to correctly capture the $n = 1$ Mott state. Such a wavefunction is given by

$$|\Psi\rangle_0 \;=\; \prod_{\Lambda=\{A,B,C,D\}} \prod_{i\in\Lambda} \times (c_{i,(n=0)}|n=0\rangle_i + |n=1\rangle_i + |n=2\rangle_i), \tag{15}$$

where

$$|n=1\rangle_i \;=\; \sum_{m=-3}^{3} c_{i,(n=1,S=3,m)} b^\dagger_{i,m}|0\rangle \tag{16}$$

and

$$\begin{aligned} |n=2\rangle_i \;&=\; \sum_{S=\{0,2,4,6\}} \sum_{m=-S}^{S} c_{i,(n=2,S,m)} |2;S,m\rangle_i \\ &=\; \sum_{S=\{0,2,4,6\}} \sum_{m=-S}^{S} c_{i,(n=2,S,m)} \\ &\quad \times \sum_{ab} \xi_{(S,a+b=m)}\; b^\dagger_{i,a} b^\dagger_{i,b}|0\rangle, \end{aligned} \tag{17}$$

where $\xi_{(S,a+b=m)}$ are Clebsch-Gordan coefficients. The normalization of $|\Psi\rangle_0$ leads to the condition

$$\begin{aligned} 1 \;&=\; |c_{i,(n=0)}|^2 + \sum_{m=-3}^{3} |c_{i,(n=1,S=3,m)}|^2 \\ &\quad + \sum_{S=\{0,2,4,6\}} \sum_{m=-S}^{S} |c_{i,(n=2,S,m)}|^2. \end{aligned} \tag{18}$$

Using this wavefunction, the expectation value of the kinetic term is given by

$$E_K \;=\; {}_0\langle\Psi|\mathcal{H}_K|\Psi\rangle_0 = -t \sum_{\langle i,j\rangle,a} 2\;\Re(\Delta^*_{ia}\Delta_{ja}), \tag{19}$$

where the superfluid order parameter $\Delta^*_{ia} = {}_0\langle\Psi|b^\dagger_{ia}|\Psi\rangle_0$ can be expressed in terms of coefficients of the variational wavefunction $|\Psi\rangle_0$ as

$$\begin{aligned} \Delta^*_{ia} \;&=\; c^*_{i,(n=1,S=3,a)} c_{i,(n=0)} \\ &\quad + \sum_{S=\{0,2,4,6\}} \sum_{m'=-S}^{S} \sum_{bc} \sum_{m=-3}^{3} c^*_{i,(n=2,S,m')} \\ &\quad \times c_{i,(n=1,S=3,m)} \xi_{(S,b+c=m')} (\delta_{ba}\delta_{cm} + \delta_{bm}\delta_{ca}). \end{aligned} \tag{20}$$

Since the interaction terms $\mathcal{H}_O$ and $\mathcal{H}_D$ (Eqs. 9 and 10) do not mix states with different n, the total variational energy can be written as

$$E_{\rm var} \;=\; E_{Mott}(n=1) + E_K + \delta E_h + \delta E_p, \tag{21}$$

where δE_p and δE_h which are the energy costs of adding a particle and hole respectively to the Mott state, are given by

$$\begin{aligned}\delta E_p &= \frac{1}{N}\Big[\langle\Psi_{\rm dipole}(n=2)| \\ &\times\Big(\mathcal{H}_O+\mathcal{H}_D-\mu\sum_i\hat{n}_i\Big)|\Psi_{\rm dipole}(n=2)\rangle \\ &-\langle\Psi_{\rm dipole}(n=1)| \\ &\times\Big(\mathcal{H}_O+\mathcal{H}_D-\mu\sum_i\hat{n}_i\Big)|\Psi_{\rm dipole}(n=1)\rangle\Big] \end{aligned} \tag{22}$$

$$\begin{aligned}\delta E_h &= -\frac{1}{N}\langle\Psi_{\rm dipole}(n=1)| \\ &\times\Big(\mathcal{H}_O+\mathcal{H}_D-\mu\sum_i\hat{n}_i\Big)|\Psi_{\rm dipole}(n=1)\rangle. \end{aligned} \tag{23}$$

The mean-field ground state of the system can now be obtained, as a function of t/U_0 and μ/U_0 for representative values of U_1/U_0, U_2/U_0, U_3/U_0 and U_4/U_0, by numerical minimization of $E_{\rm var}$. Note that as t exceeds a critical value t_c, the energy gain from E_K (Eq. 19) exceeds the energy cost of adding a particle (δE_p) or a hole (δE_h) to the Mott state. At this point, the ground state of the system occurs with non-zero superfluid order parameter $\Delta_a = \sum_i \Delta_{ia}$.

We obtain t_c by minimizing $E_{\rm var}$ (Eq. 21). In doing so, to reduce computational time, we only keep the two lowest manifolds of S states in the Mott phase corresponding to $|n=2\rangle_i$ (Eq. 17). The justification of this procedure comes from the following. At the superfluid-insulator phase boundary, the hopping coefficient t reaches a critical value for which it becomes energetically favorable to add (or remove) a particle to the $n=1$ Mott state. When such a particle is added, the resultant state has $n=2$ and can, in principle, have superposition of $S=0,2,4,6$ states due to the presence of the dipole term. However, when the dipole interaction is weak compared to the on-site interaction, such superposition becomes energetically costly. Thus the resultant lowest-energy $n=2$ state is almost entirely localized within the two lowest S manifolds for $t \simeq t_c$. We have numerically checked for a few cases keeping all the S states that this is indeed the case.

The mean-field superfluid-insulator phase boundary, so obtained, is shown in Fig. 8 for representative parameter values $U_1 = 0$, $U_2 = 0.05U_0$, $U_3 = 0.02U_0$ and $U_4 = 0.0125U_0$. Here the two lowest $n=2$ states corresponds to $S=2$ and $S=4$ manifolds and we have kept these states for our minimization calculation. We note that compared to the usual Bose-Hubbard model[3], the transition occurs for a relatively higher t_c/U. This phenomenon can be understood to be the consequence of the spin-ordering of the Mott state which originates from the dipole interaction. For sake of clarity, we shall consider the situation where the Mott state is destabilized by addition of holes. The other case, where the Mott state is destabilized by addition of particles, has a similar explanation.

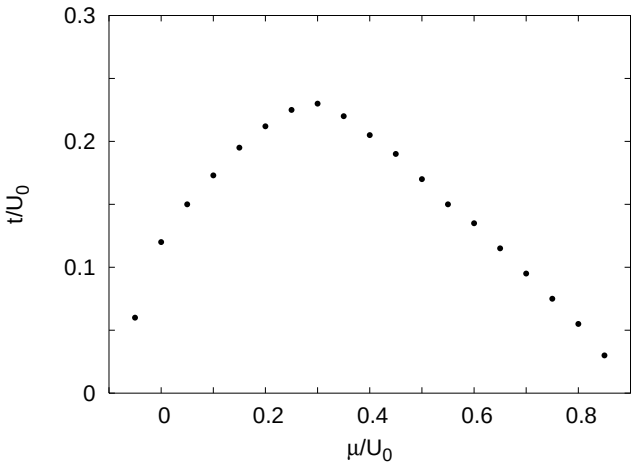

FIG. 8: The mean-field phase boundary for the superfluid-insulator transition with the $n=1$ Mott state in an optical lattice. Here $U_2 = 0.05U_0$, $U_3 = 0.02U_0$ and $U_4 = 0.0125U_0$. Notice the relatively higher values of t_c/U_0 compared to the usual cases, which is a consequence of spin order in the Mott phase (see text).

Consider the Mott state of the system with the spin order as shown in Fig. 7. It turns out that the coefficients c_i corresponding to spins in nearby chains have opposite signs because the spin directions are staggered from one chain to the other. Since $\Delta^*_{i,a} \sim c^*_{i,(n=1,S=3,a)} c_{i,(n=0)}$, the sign of Δ_i varies between different sites. Consequently, the sign of $\Delta^*_i\Delta_j$ in Eq. 19 can vary so that the kinetic energy is 'frustrated'. This leads to a reduction of the kinetic energy and hence one needs a higher t value to destabilize the Mott phase. We note that this phenomenon is generic and is a consequence of dipolar interaction between the spins, which stabilizes the above-mentioned four-sublattice order.

B. AFM-FM transition

In this section, we study the spin-ordering of the superfluid phase near the transition. The strategy for such a study is again minimization of $E_{\rm var}$ followed by computation of $\langle S_x\rangle$ and $\langle S_y\rangle$ using the variational ground state wave function. However, even before such a computation is carried out, one can guess the result from a simple physical picture, which we now present.

We have already noted in Sec. III A that the AFM spin-order along the shorter trap direction, which minimizes the dipole energy in the Mott state, is in competition with maximization of kinetic energy near the superfluid-insulator transition. Thus as we go deeper in the superfluid phase, we expect that there would be a transition from a state with such a spin-order to a FM state where all the spins point towards x (the longer trap direction). Such a transition from the translational-symmetry bro-

ken AFM state to a uniform FM state is expected to be first order. The exact location of this transition depends on the relative strength of t, μ and U_4. As shown in Fig. 9, the AFM-FM transition follows closely the MI-SF transition for values of μ/U_0 smaller than $(\mu/U_0)_{t_c^{\max}}$ and departs from the MI-SF transition boundary for larger values of μ/U_0. This departure from the MI-SF boundary can be explained by noticing that the Mott state is destabilized primarily by addition of holes (particles) for μ/U_0 close to 0(1). For intermediate values of μ, the destabilization of the Mott phase occurs, within mean-field theory, with finite amplitudes for addition of both holes and particles. Consequently, for a fixed μ/U_0 close to 0, as we increase t/U_0, the average number of bosons per site decreases and $\langle S_x \rangle$ decreases accordingly. Therefore, the effective dipole interaction becomes weaker and $t_{\rm afm}$, the value of t for which the kinetic energy gain wins over the optimization of the dipolar energy, stays close to t_c. However, for a fixed μ/U_0 close to 1, the average number of bosons per site increases as t is increased beyond t_c and $\langle S_x \rangle$ also slowly increases. Thus, for $\mu > \mu_{t_c^{\max}}$, the dipole interaction is robust to an increase in t/U_0 so that $t_{\rm afm}$ becomes larger and deviates significantly from the Mott-superfluid phase boundary.

We have also computed the variation of $t_{\rm afm}$ with U_4, as shown in Fig. 10 for representative values of parameters $U_3 = 0.02U_0$, $U_2 = 4U_4$ and $\mu = 0.05U_0$. We find that $t_{\rm afm}$ approaches t_c for small values of U_4/U_0. The AFM-FM transition occurs simultaneously with the MI-SF transition for $U_4 \leq 0.00125U_0$, leading to a first order MI-SF transition in this regime. Such dependence of $t_{\rm afm}$ on U_4 can be understood by noting that a reduction of U_4 directly decreases the dipolar energy. As a result, when U_4 is reduced, the AFM spin ordering becomes less robust to increases in t because it becomes easier to take advantage of the kinetic energy gain at the expense of the dipolar energy. Thus $t_{\rm afm}$ decreases, and ultimately merges to t_c for $U_4/U_0 \leq 0.00125$.

Finally, we investigate the fate of the spin-order as we go deeper in the SF region. We note at the outset that since the approximation involved in our minimization scheme loses its accuracy as we go deeper into the superfluid phase, we do not expect our analysis to be quantitatively accurate in this regime, but only expect some qualitative features to be captured. To this end, we plot $\langle S_x \rangle$ as a function of t/U_0 with $\mu/U_0 = 0.05$ (with all other parameters being the same as in Fig. 8) as shown in Fig. 11. Note that here $t_c \simeq 0.16U_0$ and $t_{\rm afm} \simeq 0.17U_0$, so that t_c and $t_{\rm afm}$ are quite close to each other. As we further increase t, we find that for $t/U_0 \geq 0.27$, we have a transition to the paramagnetic phase where $\langle S_x \rangle = 0$. We have also computed the expectation value of the nematic order parameters in the FM state. The results of these computation are summarized in Fig. 12. We find that for $t \leq 0.23U_0$ and $t \geq 0.27U_0$, we have a uniaxial nematic phase. For $0.23 < t/U_0 < 0.27$, in the region over which $\langle S_x \rangle$ decrease from its maximum value to 0, we find a biaxial nematic phase, similar to one found in Ref. 15. However, we note that at the point where the biaxial nematicity sets in, we are already deep inside the SF phase and our approximations of retaining the two lowest manifold of states may be inaccurate.

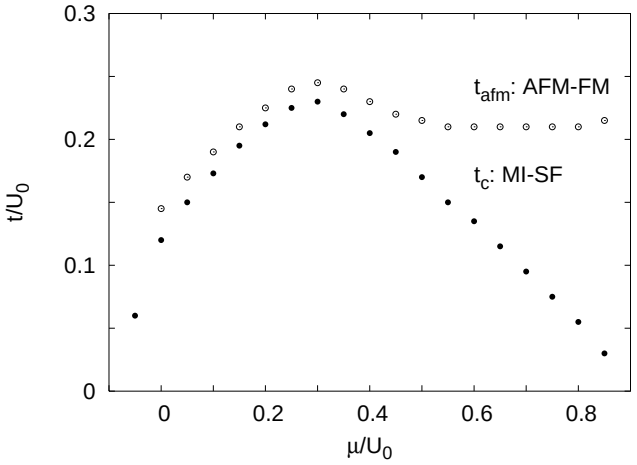

FIG. 9: The AFM-FM and the MI-SF transition boundaries for the $n = 1$ Mott state in an optical lattice as a function of μ/U_0. Here $U_2 = 0.05U_0$, $U_3 = 0.02U_0$ and $U_4 = 0.0125U_0$. Notice that the AFM-FM transition follows closely the MI-SF transition for values of μ/U_0 smaller than $(\mu/U_0)_{t_c^{\max}}$ and departs from the MI-SF transition boundary for larger values of μ/U_0.

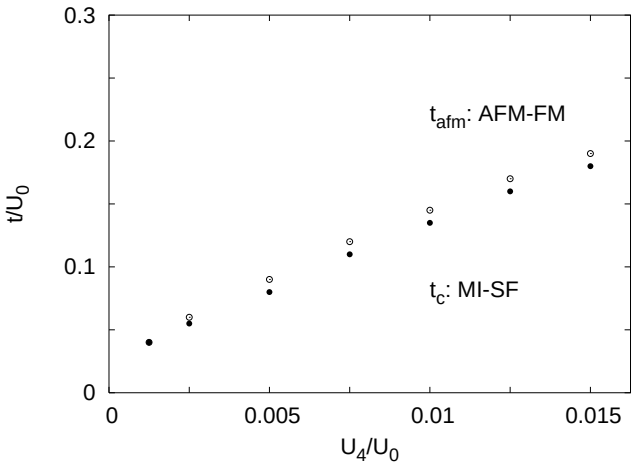

FIG. 10: The AFM-FM and the MI-SF transition boundaries for the $n = 1$ Mott state in an optical lattice as a function of U_4/U_0 for $U_3 = 0.02U_0$, $U_2 = 4U_4$ and $\mu = 0.05U_0$. Notice that for $U_4 = 0.00125U_0$, the AFM-FM transition occurs simultaneously with the MI-SF transition.

IV. EXPERIMENTS

The traditional way of examining the existence of superfluidity in trapped boson systems is to switch off the trap, let the cloud of atoms expand freely and image the expanding cloud. The momentum distribution of

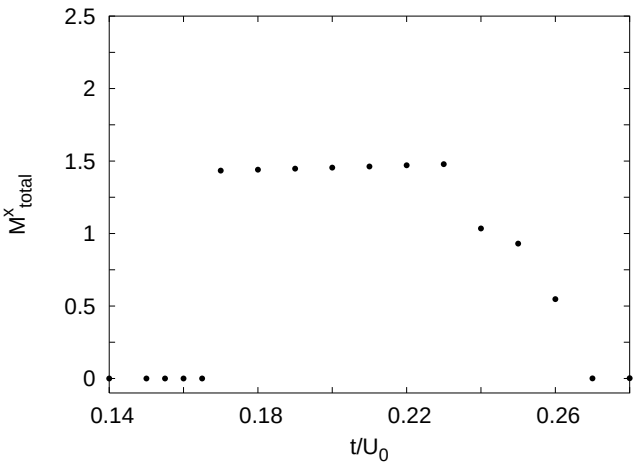

FIG. 11: Total magnetization in the x direction ($M^x_{\rm total} = \langle \sum_i S^x_i \rangle / N$, where the sum is over all lattice sites) for the Mott and superfluid phases as a function of t/U_0. Here $\mu = 0.05U_0$, $U_2 = 0.05U_0$, $U_3 = 0.02U_0$, and $U_4 = 0.0125U_0$. Note that the AFM-FM transition occurs for $t_{\rm afm} \simeq 0.17U_0 > t_c \simeq 0.16U_0$ and, as we increase t, the FM order gives away to a paramagnetic superfluid for $t > 0.27U_0$.

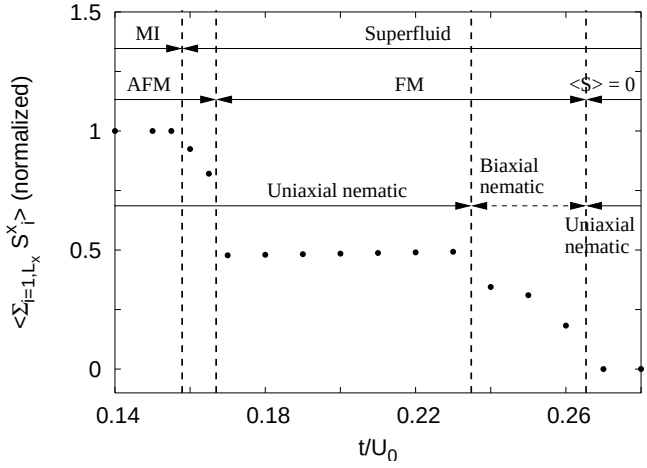

FIG. 12: AFM, FM, superfluid and nematic phases as a function of t/U_0 for $\mu = 0.05U_0$, $U_2 = 0.05U_0$, $U_3 = 0.02U_0$ and $U_4 = 0.0125U_0$. Here we have plotted $\langle \sum_{i=1,L_x} S^x_i \rangle / (3N_x)$, where the sum is over the N_x number of sites in a given chain along the x direction (the longer trap direction). It turns out that its magnitude in the superfluid phase varies with μ and the U's.

the atoms inside the trap can then be inferred by looking at their position, or equivalently density, distribution in the expanded cloud. Since the momentum distribution function of the atoms is characterized by the presence/absence of coherence peaks in the superfluid/Mott insulating states, such a measurement serves as a qualitative probe of the state of the atoms inside the trap[1]. In our proposed setup, however, such a simple expansion alone, which is not sensitive to the different spin states of atoms, will not be able to distinguish between all the different phases. To achieve this distinction, we need to use the well-known technique of passing the expanding cloud through a Stern Gerlach magnet with the magnetic field along y (shorter trap direction)[4,5]. Such a Stern-Gerlach magnet will split the expanding cloud into two clouds of equal proportion if the atoms in the trap were in the AFM phase. If the atoms were in the FM phase, no such splitting will occur. Thus, a momentum-distribution measurement, along with the Stern Gerlach measurement described above can distinguish between the Mott-AFM (delocalized momentum distribution and two clouds), superfluid-AFM (localized momentum distribution and two clouds) and superfluid-FM phases (localized momentum distribution and single cloud). However, we note that such measurements do not uniquely determine the details of the spin configuration in the AFM state. The signature of the details of the spin configuration can be obtained experimentally by measuring the spatial noise correlations of the expanding clouds[20]. Finally, the uniaxial and biaxial nematic orders can also be detected using an imaging technique suggested in Ref. 21.

V. CONCLUSION

In conclusion, we have studied the Mott insulating phases and superfluid-insulator phase transitions of $S = 3$ bosons in an optical lattice. In particular, we have considered dipolar interaction between the bosons and the effect of rectangular optical trap. We have investigated possible Mott phases of such systems for integer $n = 1$ and $n = 2$ atoms per lattice site and shown that the presence of dipolar interaction leads to a state with ferromagnetic chains along the longer trap direction which are aligned antiparallel to each other, thus leading to an antiferromagnetic order along the shorter trap direction. We have also presented a mean-field phase diagram for the superfluid-insulator transition in these systems and have shown that there is a generic first order AFM-FM transition in the superfluid region close to the superfluid-insulator phase boundary. We have also suggested realistic experiments on ^{52}Cr to verify our predictions.

Acknowledgments

This work was supported by NSERC, the Canada Research Chair Program, the Canadian Institute for Advanced Research, KRF-2005-070-C00044 (J.S.B. and Y.B.K.), Le Fonds Québécois de la Recherche sur la Nature et les Technologies (J.S.B.) and the Miller Institute of Basic Research in Science at UC Berkeley via the Visiting Miller Professorship (Y.B.K.).

APPENDIX A: COMPUTATION OF THE VARIATIONAL ENERGY FOR THE MOTT PHASES

We present in this section the expression of the variational energy $E_v(n)$ (Eq. 11) in greater detail. Following Eq. 9, the on-site energy is given by

$$\begin{aligned} E_v(n) &= \langle\Psi_v(n)|\,\{\ \frac{U_0}{2}\sum_i \hat{n}_i(\hat{n}_i-1) \\ &+\ \frac{U_2}{2}\sum_i(\mathbf{S}_i^2-12\ \hat{n}_i) \\ &+\ \frac{U_1}{2}\sum_i\sum_{ab}\frac{1}{7}(-1)^a\ b_{ia}^\dagger\ b_{i-a}^\dagger\ (-1)^b\ b_{ib}\ b_{i-b} \\ &+\ \frac{U_3}{2}\sum_i\ [\sum_{k,l=\{x,y,z\}} N_{i,kl}^2-132\ \hat{n}_i] \\ &-\ \mu\ \hat{n}_i\ \}\,|\Psi_v(n)\rangle\,. \end{aligned} \tag{A1}$$

To compute the on-site energy in the case of $n=1$, we use the variational wavefunction

$$|\Psi_v(1)\rangle = \prod_i \sum_{m=-3}^{3} c_{i,(n=1,S=3,m)} b_{i,m}^\dagger|0\rangle, \tag{A2}$$

while for $n=2$, we use

$$\begin{aligned} |\Psi_v(2)\rangle &= \prod_i \sum_{S=\{0,2,4,6\}} \sum_{m=-S}^{S} c_{i,(n=2,S,m)} \\ &\times \sum_{ab}\ \xi_{(S,a+b=m)}\ b_{i,a}^\dagger\ b_{i,b}^\dagger|0\rangle, \end{aligned} \tag{A3}$$

where $\xi_{(S,a+b=m)}$ are Clebsh-Gordan coefficients. Using these wavefunctions, we find the energies for $n=1$ and $n=2$. For $n=1$, the on-site energy is given by

$$E_v(1) = -\mu\sum_i\sum_{m=-3}^{3}|c_{i,(n=1,S=3,m)}|^2, \tag{A4}$$

while for $n=2$ the energy is given by

$$\begin{aligned} E_v(2) &= \sum_i\ \{(U_0-2\ \mu)\ \sum_S\sum_{m=-S}^{S}|c_{i,(n=2,S,m)}|^2 \\ &+\frac{U_2}{2}\sum_S\sum_{m=-S}^{S}|c_{i,(n=2,S,m)}|^2(S(S+1)-24) \\ &+U_1\ |c_{i,(n=2,S=0,m=0)}|^2 \\ &+\frac{U_3}{2}(288\ |c_{i,(n=2,S=0,m=0)}|^2 \\ &\quad+162\sum_{m=-2}^{2}|c_{i,(n=2,S=2,m)}|^2 \\ &\quad+8\sum_{m=-4}^{4}|c_{i,(n=2,S=4,m)}|^2 \\ &\quad+162\sum_{m=-6}^{6}|c_{i,(n=2,S=6,m)}|^2)\}. \end{aligned} \tag{A5}$$

The Mott phases are then obtained by minimizing $E_v(n)$ with respect to the variational parameters $c_{i,(n,S,m)}$.

[1] M. Greiner, O. Mandel, T. Esslinger, T.W. Hänsch and I. Bloch, Nature **415**, 39 (2002).

[2] C. Orzel, A.K. Tuchman, M.L. Fenselau, M. Yasuda and M.A. Kasevich, Science **291**, 2386 (2001).

[3] M.P.A. Fisher, P.B. Weichman, G. Grinstein, and D.S. Fisher, Phys. Rev. B **40**, 546 (1989).

[4] J. Stenger, S. Inouye, D.M. Stamper-Kurn, H.-J. Miesner, A.P. Chikkatur, W. Ketterle, Nature **396**, 345 (1998).

[5] A. Widera, F. Gerbier, S. Fölling, T. Gericke, O. Mandel and I. Bloch, Phys. Rev. Lett. 95, 190405 (2005); A. Widera, F. Gerbier, S. Fölling, T. Gericke, O. Mandel and I. Bloch, New J. Phys **8**, 152 (2006).

[6] L.-M. Duan, E. Demler, and M. D. Lukin, Phys. Rev. Lett. **91**, 090402 (2003); E. Altman, W. Hofstetter, E. Demler, and M.D. Lukin, New J. Phys. **5**, 113 (2003).

[7] A. Isacsson, M-C Cha, K. Sengupta and S.M. Girvin, Phys. Rev. B **72**, 184507 (2005).

[8] F. Zhou and G. W. Semenoff, Phys. Rev. Lett. **97**, 180411 (2006).

[9] S. Powell and S. Sachdev, cond-mat/0608611.

[10] R. Barnett, A. Turner and E. Demler, Phys. Rev. Lett. **97**, 180412 (2006); R. Barnett, A. Turner and E. Demler, cond-mat/0611230; S.-K. Yip, cond-mat/0611171.

[11] A. Imambekov, M. Lukin, and E. Demler, Phys. Rev. A **68**, 063602 (2003); J.-S. Bernier, K. Sengupta and Y.B. Kim, Phys. Rev. B **74**, 155124 (2006).

[12] J.-M. Hou and M.-L. Ge, Phys. Rev. A **67**, 063607 (2003).

[13] A. Griesmaier, J. Werner, S. Hensler, J. Stuhler and T. Pfau, Phys. Rev. Lett **94**, 160401 (2006).

[14] J. Stuhler, A. Griesmaier, T. Koch, M. Fattori, T. Pfau, S. Giovanazzi, P. Pedri and L. Santos, Phys. Rev. Lett **95**, 150406 (2005).

[15] R.B. Diener and T-L. Ho, Phys. Rev. Lett. **96**, 190405 (2006).

[16] L. Santos and T. Pfau, Phys. Rev. Lett. **96**, 190404 (2006).

[17] Refs. 15 and 16 differ regarding the presence of a biaxial nematic phase, but agree on the presence of more common uniaxial nematic phases in these systems.

[18] D. Jaksch, C. Bruder, J.I. Cirac, C.W. Gardiner and P. Zoller, Phys. Rev. Lett. **81**, 3108 (1998).

[19] C. Schroll, F. Marquadt, and C. Bruder, Phys. Rev. A **70**, 053609 (2004).

[20] E. Altman, E. Demler, and M.D. Lukin, Phys. Rev. A **70**, 013603 (2004).

[21] I. Carusotto and E. Mueller, J. Phys. B **37**, S115 (2004).